American Mineralogist, Volume 84, pages 435–446, 1999

Laplacian and bond critical point properties of the electron density distributions of sulfide bonds: A comparison with oxide bonds*

G.V. Gibbs,[1,*] Osamu Tamada,[2] M.B. Boisen Jr.,[3] and F.C. Hill[3]

[1]Departments of Geological Sciences, Materials Science and Engineering and Mathematics, Virginia Tech, Blacksburg, Virginia 24061 U.S.A.
[2]Graduate School of Human and Environmental Studies, Kyoto University, Kyoto 606, Japan
[3]Departments of Mathematics and Geological Sciences, Virginia Tech, Blacksburg, Virginia 24061 U.S.A.

Abstract

Topological and bond critical point properties of electron density distributions, $\rho(\mathbf{r})$, were calculated for a series of sulfide molecules, containing first- and second-row main group M-cations. Laplacian maps of the distributions, $\nabla^2\rho(\mathbf{r})$, show that the valence shell charge concentration (VSCC) of the sulfide anion is highly polarized and extended into the internuclear region of the M-S bonds, coalescing with the VSCCs of the more electronegative first-row cations. On the other hand, maps for a corresponding set of oxide molecules show that the oxide anion tends to be less polarized and more locally concentrated in the vicinity of its valence shell, particularly when bonded to second-row M-cations. A search for extrema in the $\nabla^2\rho(\mathbf{r})$ distributions reveals maxima in the VSCCs that can be ascribed to bonded and nonbonded electron pairs. The different and distinctive properties of sulfides and oxides are examined in terms of the number and the positions of the electron pairs and the topographic features of the Laplacian maps. The evidence provided by the electron density distributions and its topological properties indicates that the bonded interactions in sulfides are more directional, for a given M-cation, than in oxides. The value of the electron density distribution at the bond critical point and the length of a given M-S bond are reliable measures of a bonded interaction, the greater the accumulation of the electron density and the shorter the bond, the greater its shared (covalent) interaction.

Introduction

The sulfide anion differs from its congener oxide anion in several distinctive ways: (1) the radial probability density distribution of its valence orbitals is relatively diffuse and extended in space whereas that of the oxide anion is more localized in a region closer to the anion; (2) its dipole polarizability is roughly four times larger than that of the oxide anion; (3) its radius is larger; and (4) its electronegativity is smaller (Kutzelnigg 1984). Given these differences, it is not surprising that the crystal chemistry of the sulfides is different and distinct from that of the oxides (Wuench 1974). As one example, silicates and thiosilicates differ in several important ways: (1) silicates are common and widespread in nature whereas thiosilicates have yet, to our knowledge, to be reported as naturally occurring minerals, (2) silicates crystallize with a wide variety of structure types whereas thiosilicates adopt a much more limited variety of structures, (3) silicates with condensed tetrahedra exhibit a relatively wide range of bridging Si-O-Si angles (120–180°) whereas thiosilicates exhibit a much more restricted range (105–115°), and (4) SiO_2 is a good glass-forming material whereas the glass forming tendencies of SiS_2 are not as good (cf. Geisinger and Gibbs 1981; Kaftory et al. 1998 and references therein). On the other hand, despite the observation that the quadratic force constant of the longer Si-S bond (~300 N/m) is smaller than that of a comparable Si-O bond (~600 N/m), the range of Si-S bond lengths (2.02 to 2.21 Å) recorded for the thiosilicates is similar to that recorded for the silicates (1.57 to 1.72 Å; Liebau 1985; Gibbs et al. 1987a; Hill et al. 1994; Kaftory et al. 1998). In addition, the bond lengths calculated for oxide and sulfide molecules containing main group M-cations match those observed for crystals fairly well (Gibbs et al. 1987b; Bartelmehs et al. 1989). These bond lengths, R, also correlate with the strength of the bonds, p, [$p = s/r$ where s is the Pauling (1929) bond strength and r is the row number of the M-cation] according to the power law expression $R = \alpha p^{-\beta}$ where $\beta \sim .22$ and $\alpha = 1.39$ and 1.84, respectively, for M-O and M-S bonds (Gibbs et al. 1987b; Bartelmehs et al. 1989). In a study of the power law relationship between p and the accumulation of electron density along the bonds in oxide molecules and crystals, Gibbs et al. (1998b) found that p correlates with the average value of the electron density, $\rho(\mathbf{r}_c)$, at the bond critical points, $\mathbf{r}_c$, of the M-O bonds forming the coordinated polyhedra in these materials, the larger the value of p, the greater the average value of

* E-mail: gvgibbs@vt.edu

0003–004X/99/0003–0435$05.00

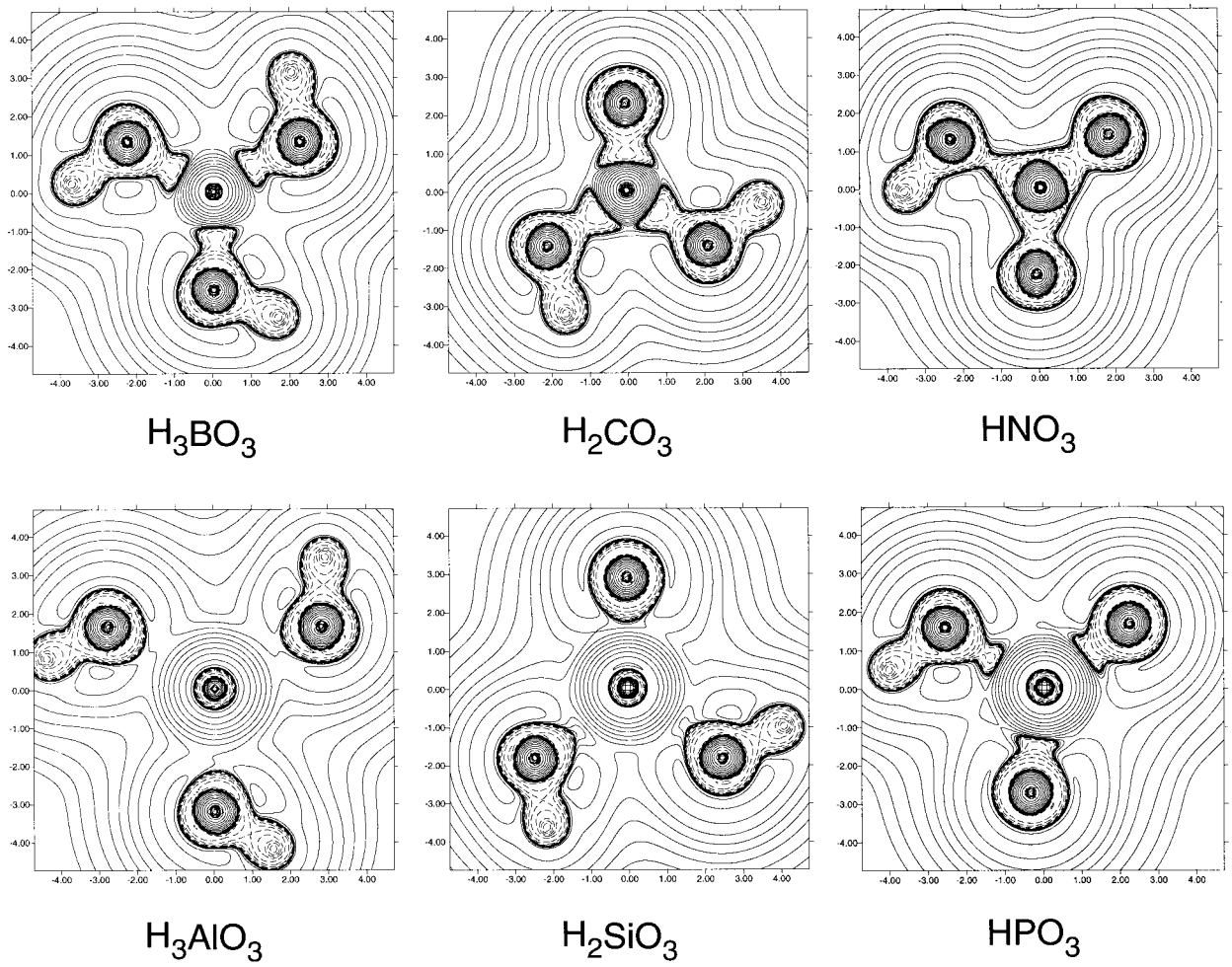

FIGURE 1. Laplacian maps of the electron density distribution calculated for $H_{6-n}M^{+n}O_3$ molecules, M = B, C, N, Al, Si, and P. The M-cation is located at the center of each molecule, and H atoms are attached to the oxide anions to achieve electrical neutrality. The solid lines represent positive $\nabla^2\rho(r)$ level lines, and the dashed ones represent negative $\nabla^2\rho(\mathbf{r})$ level lines. The level line intervals increase and decrease from the zero level in stages of $\pm 2 \times 10^n$, $\pm 4 \times 10^n$, $\pm 8 \times 10^n$, . . ., beginning at $n = -3$.

$\rho(\mathbf{r}_c)$. The average bond lengths recorded for the coordinated polyhedra decrease monotonically with increasing electron density as defined by a power law relationship with the same exponent, ~0.22.

A mapping of the electron density distributions, $\rho(\mathbf{r})$, calculated for the M-O bonds of a relatively large number of oxide molecules was recently undertaken in an exploration of their bond critical point, bcp, properties (Gibbs et al. 1994; Gibbs et al. 1997; Hill et al. 1997; Gibbs et al. 1998a). In these studies, the properties were examined as the electronegativities of first- and second-row M-cations increase from left to right in the periodic table. They were also found to agree with those observed and calculated for crystals to within ~5%, on average (Gibbs et al. 1998a; Rosso et al. 1998). As the molecules and crystals exhibit a relatively wide range of bond types that encompass shared (covalent), intermediate and closed-shell (ionic) bonded interactions, the study afforded an opportunity to evaluate the bcp properties of the electron density distributions together with the optimized geometries of the molecules in terms of sets of rules forged by Bader and Essën (1984) and Cremer and Kraka (1984) for classifying bond type. In our study, the Laplacian of the valence electron density distributions and the bcp properties of M-S and M-O bonds will be compared and discussed in terms of the geometry-optimized bond lengths, the electronegativities of the M-cations and the Bader-Essën and Cremer-Kraka rules for classifying bond type. The maxima in the VSCCs of the sulfide and oxide anions will likewise be located in an effort to further our understanding of why the crystal chemistries of sulfides and oxides are different and distinctive at the microscopic level.

Laplacian distributions of selected sulfide and oxide molecules

In a series of groundbreaking papers on molecular structure and chemical bonding, Bader (1990) and his

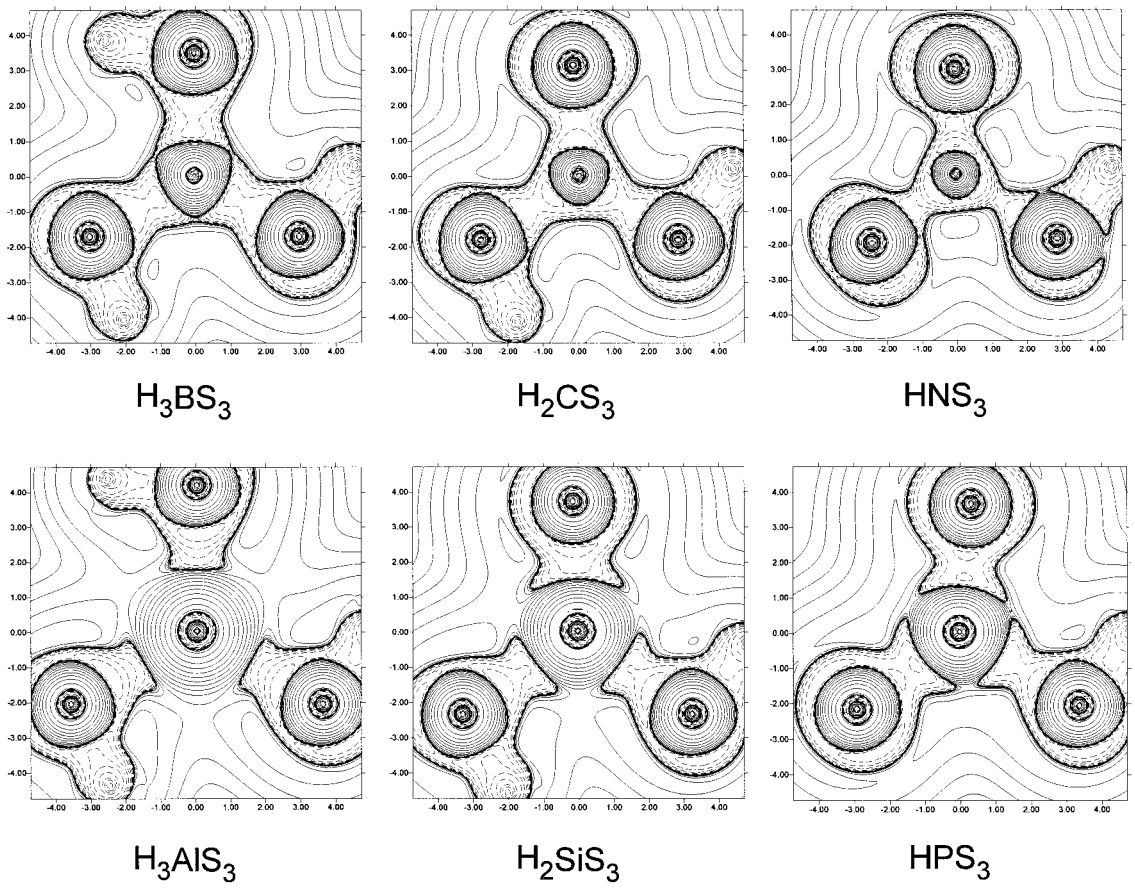

FIGURE 2. Laplacian maps of the electron density distribution calculated for $H_{6-n}M^{+n}S_3$ molecules. See legend for Figure 1 for details.

colleagues have argued that the atomic interactions present in molecular systems can be identified, assessed, and characterized by the gradient, $\nabla\rho(\mathbf{r})$, and the Laplacian, $\nabla^2\rho(\mathbf{r})$, of their electron density distributions (Bader et al. 1981; Bader et al. 1984; Bader and Essën 1984; MacDougall 1989). For example, $\nabla\rho(\mathbf{r})$ can be used to define the atoms and the structure of a molecule or a crystal. It can be also used to define a chemical bond, a concept that has been traditionally regarded as undefined and therefore an unobservable. Based on experience gained from studies of the gradient vector field of $\rho(\mathbf{r})$, each pair of bonded atoms in a minimum energy equilibrium molecule was defined to be bonded whenever the pair is connected by a unique line in the field along which the electron density is a maximum with respect to any neighboring line (Bader and Essën 1984). Such a line was defined by Bader (1990) to be the atomic interaction line referred to simply as the bond path (Bader and Essën 1984; Cremer and Kraka 1984). The formation of a bond path indicates that there has been an accumulation of electron density between the nuclei of the bonded atoms, a necessary condition for bond formation. As such the path manifests itself in an electron density map through a pair of bonded atoms as a ridge of electron density. The point along the top of the ridge where $\rho(\mathbf{r})$ is a minimum defines a $(3,-1)$ bond critical point (a saddle point in the electron density distribution), $\mathbf{r}_c$, where $\nabla\rho(\mathbf{r}) = 0$; the line that runs along the top of the ridge delineates the bond path. The absence of such a line between a pair of adjacent atoms in a molecule or crystal is taken as evidence that a chemical bond is absent and that the atoms are nonbonded. The point, $\mathbf{r}_c$, where $\nabla\rho(\mathbf{r})$ vanishes is characterized by three curvatures of $\rho(\mathbf{r})$ along three mutually perpendicular directions; $|\lambda_1|$ and $|\lambda_2|$ denote the curvatures of $\rho(\mathbf{r}_c)$ measured in two mutually perpendicular directions perpendicular to the bond path and λ_3 denotes the curvature at $\mathbf{r}_c$ measured along the path. With decreasing bond length and increasing $\rho(\mathbf{r}_c)$, $|\lambda_1|$, and $|\lambda_2|$ typically increase as the negative curvatures of $\rho(\mathbf{r}_c)$ perpendicular to the path sharpen; as λ_3 increases, the positive curvature of $\rho(\mathbf{r}_c)$ along the path sharpens, a feature that can, as a rule, be associated with a shortening of the bond (Hill et al. 1997; Feth et al. 1998). As shown by Bader (1990), $\nabla^2\rho(\mathbf{r}_c)$ is directly related to the curvatures of $\rho(\mathbf{r})$ by the expression $\nabla^2\rho(\mathbf{r}_c) = \lambda_1 + \lambda_2 + \lambda_3$, the trace of the Hessian of $\rho(\mathbf{r}_c)$. Also, $\nabla^2\rho(\mathbf{r}_c)$ delineates those regions where $\rho(\mathbf{r})$ is locally greater or less than its average value in the vicinity of **r.** Regions where $\nabla^2\rho(\mathbf{r})$ is nega-

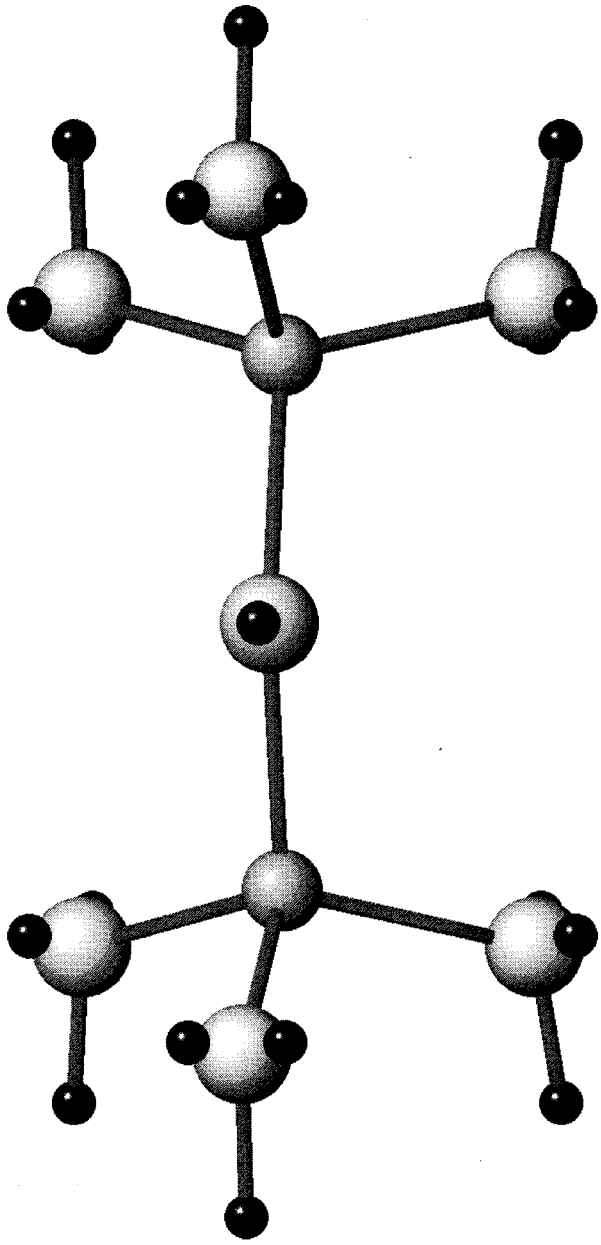

FIGURE 3. A drawing of the $H_6Si_2O_7$ molecule (geometry optimized assuming C_{2v} point symmetry) and the local concentration maxima (3,−3) critical points associated with VSCC of each O atom. The points are depicted by the small darker gray spheres, the large spheres represent O, the dark intermediate sized spheres represent Si, and smaller gray spheres attached by a rod to each O represents a H atom. The bridging O atom displays one (3,−3) in its VSCC and each nonbridging O displays two, each ascribed a local concentration of lone pair (lp) density (the (3,−3) local concentrations ascribed to the bond pairs are not shown). The lp associated with the bridging O is at a distance of 0.350 Å from the O atom and the lp-O-Si angle is 105.43°. The two lps on each nonbridging O are each at a distance of 0.346 Å from the atom, the lp-O-lp angle is 105.29° and both lp-O-H angles are 105.48°.

tive, the electron density is locally greater than the average value in the immediate vicinity of **r**; $\rho(\mathbf{r})$ in these regions is said to be locally concentrated. In contrast for regions where $\nabla^2\rho(\mathbf{r})$ is positive, the electron density is locally less than the average value in the immediate vicinity of **r**; $\rho(\mathbf{r})$ is said to be locally depleted or expanded in these regions. However, it does not necessarily follow that either an overall accumulation or a loss of electron density exists in the region of **r** when the sign of $\nabla^2\rho(\mathbf{r})$ is either negative or positive. As observed above, as electron density accumulates at the critical point, $|\lambda_1|$ and $|\lambda_2|$ increase and $\rho(\mathbf{r})$ is said to be contracted toward the bond path. On the other hand, as λ_3 increases, $\rho(\mathbf{r})$ expands away the interatomic surface (the surface that is generated by the set of all gradient paths that terminate at $\mathbf{r}_c$) and that separates the basins of the two atoms (Bader and Essën 1984). The basin of an atom is defined to be the region of space traversed by the set of all of the trajectories of $\nabla\rho(\mathbf{r})$ that terminate at the nucleus of an atom. Within this context, an atom is defined to be the union of the nucleus (the attractor) and its associated basin.

The electron density distribution of an isolated atom is characterized by a single maximum that decays exponentially with distance from the atom, whereas the Laplacian of the distribution consists of series of concentric, alternating shells where the electron density is locally concentrated and locally depleted, features that reflect the shell structure of the atom with the outermost shell corresponding to the valence shell. This shell is referred to as the valence shell charge concentration of the atom (Bader. 1990).

The formation of a chemical bond and the interatomic surface between a pair of bonded atoms is asserted by Bader (1990) to result from the competition between the contraction of the electron density perpendicular to the path and the expansion of the density away from the interatomic surface into the basins of the atoms. Upon chemical combination and bond formation, atoms interact and their VSCCs are distorted to one degree or another, depending on the nature and the extent of the interaction. In a study of the interactions displayed by a variety of molecules, Bader and Essën (1984) established a set of criteria for classifying the interaction between a pair of bonded atoms in terms of the value of $\rho(\mathbf{r}_c)$ and the properties and spatial distribution of $\nabla^2\rho(\mathbf{r})$ in the valence shell and internuclear regions. For a shared interaction, the value of $\rho(\mathbf{r})$ is pictured as being relatively large at $\mathbf{r}_c$ and as locally concentrated in the binding region between the bonded atoms. In addition, the region where $\nabla^2\rho(\mathbf{r})$ is negative includes the internuclear region as well as the valence shell regions of both atoms forming a contiguous domain of local charge concentration that encompasses the interatomic surface. For a closed-shell interaction, the value of $\rho(\mathbf{r}_c)$ is pictured as being relatively small with the region of local charge concentration being confined, for the most part, to the valence shell of the more electronegative atom. Also, $\nabla^2\rho(\mathbf{r})$ is pictured as being positive over much of the internuclear region including $\mathbf{r}_c$ but

negative in the region of the valence shell of the more electronegative atom where the electron density is locally concentrated. For an intermediate interaction, the value of $\rho(\mathbf{r}_c)$ is pictured as adopting an intermediate value between that of a shared and a closed shell interaction. In addition, the negative region of $\nabla^2\rho(\mathbf{r})$ is pictured as extending into the internuclear region away from the valence shell of the more electronegative atom such that the nodal surface [the $\nabla^2\rho(\mathbf{r}) = 0.0$ surface] is in close proximity with the interatomic surface. As the shared interaction increases, $\rho(\mathbf{r}_c)$ increase monotonically in value as the nodal surface of the Laplacian works its way into the valence region of the more electropositive atom and the VSCCs of the two atoms ultimately coalesce and form a contiguous region of local charge concentration that includes the internuclear as well as the valence regions of both atoms. Also, the sign of $\nabla^2\rho(r)$ should change from positive to negative as $\nabla^2\rho(\mathbf{r})$ decreases and $\rho(\mathbf{r}_c)$ increases in value.

Because M-S bonds are considered to exhibit a more shared interaction than M-O bonds for a given M cation and because the valence electrons of the sulfide anion are more polarizable and extended in space than those of the oxide anion (Bader et al. 1984), $\nabla^2\rho(r)$ maps were calculated for six planar $H_{6-n}M^{+n}O_3$ and $H_{6-n}M^{+n}S_3$ molecules containing first-row (M = B, C, and N) and second-row (M = Al, Si, and P) main group M-cations for purposes of comparison. The geometry of each of the molecules was optimized at the Becke3lyp/6–311G(2d,p) level, a hybrid method that includes a mixture of Hartree-Fock exchange with density functional theory electron exchange and non-local correlation (Frisch et al. 1993). Maps of $\nabla^2\rho(\mathbf{r})$ for the six oxide molecules are displayed in Figure 1 and those for the six sulfide molecules are displayed in Figure 2.

As the electronegativities of the M-cations of the $H_{6-n}M^{+n}O_3$ molecules increase in the first row from left to right in the periodic table from B to N, the maps show (Fig. 1), as observed for a set of diatomic hydride molecules studied by Bader and Essën (1984), a progressive invasion of the negative region of $\nabla^2\rho(\mathbf{r})$ from the region of the VSCC of the more electronegative anion into the internuclear region beyond the bond critical point $\mathbf{r}_c$ with the nodal surface completely merging with the VSCC of the N-cation as the shared component of the bonded interactions increases (Bader 1990). Accompanying this change, the $\rho(\mathbf{r}_c)$ values for the M-OH bonds of the H_3BO_3, H_2CO_3, and HNO_3 molecules increase in the order 1.45, 2.10, and 2.15 e/Å^3. In contrast, the maps calculated for the $H_{6-n}M^{+n}S_3$ molecules (Fig. 2), with the same first-row M-cations, reveal that the VSCC of the sulfide anion is highly polarized and much more extended into the internuclear region than observed for the oxide anion in Figure 1. In fact, each of the first-row cations in Figure 2 is completely enveloped by the negative region of $\nabla^2\rho(\mathbf{r})$ with the domains of the VSCCs of the metal atoms increasing in size from left to right in the periodic table as the size of the M-cation decreases. The $\rho(\mathbf{r}_c)$ values for the M-SH bonds of the H_3BS_3, H_2CS_3, and HNS_3 molecules tend to increase, 1.04, 1.36, and 1.16 e/Å^3, respectively, but in a less regular way with electronegativity than those for the M-OH bonds. This trend in $\rho(\mathbf{r}_c)$ can be related to the lengths of the M-SH bonds [R(BS) = 1.82 Å, R(CS) = 1.75 Å, R(NS) = 1.78 Å with the shortest bond displaying the largest $\rho(\mathbf{r}_c)$ value] and the fact that the electronegativity of N is substantially larger than that of the S and plays the role of the anion in the HNS_3 molecule.

For the larger second-row cations (Al, Si, and P), the negative region of $\nabla^2\rho(\mathbf{r})$ is more restricted for both the oxide and sulfide anions with the VSCCs polarized to a much lesser degree, particularly for the smaller and more electronegative oxide anion. For Al-O and Si-O bonds, the negative region of the Laplacian shows little polarization and is restricted almost entirely to the region of the valence shell of the oxide anion. In contrast, the VSCC of the oxide anions of the HPO_3 molecule is polarized into the internuclear region. The values of $\rho(\mathbf{r}_c)$ for the M-OH bonds for the H_3AlO_3, H_2SiO_3, and HPO_3 molecules also increase in a regular way (0.73, 1.00, and 1.68 e/Å^3) respectively, as their bond lengths decrease from 1.70 to 1.62 to 1.59 Å, respectively, and as the electronegativity of the M cation increases from left to right in the periodic table.

The VSCC of the sulfide anion is more highly polarized than the oxide anion even when bonded to larger, less electronegative second-row cations. For the P-S bond, the VSCC of the sulfide anion is polarized and extends into the internuclear beyond $\mathbf{r}_c$ and merges with that of the P cation. The VSCC of the sulfide anion is also polarized into the internuclear region of the Si-S and Al-S bonds but to a lesser degree. For the three molecules H_3AlS_3, H_2SiS_3, and HPS_3, the $\rho(\mathbf{r}_c)$ values for the M-SH bonds also increase regularly (0.49, 0.70, and 1.16 e/Å^3, respectively). The bond lengths for these molecules also decrease with increasing $\rho(\mathbf{r}_c)$.

The Laplacian distributions of the electron density for the two sets of molecules are consistent with the argument that the VSCC of the larger, less electronegative sulfide anion is much more extended and polarizable in space than that on the smaller, more electronegative oxide anion for which the electrons are more locally concentrated and difficult to polarize. It also indicates that bonds involving the smaller, first-row cations exhibit a larger accumulation of electron density at $\mathbf{r}_c$ than those involving second row cations as observed by Bader (1990) with $\rho(\mathbf{r}_c)$ tending to increase with increasing electronegativity and decreasing bond length. Also, $\nabla^2\rho(\mathbf{r}_c)$ tends to decrease and become negative as $\rho(\mathbf{r}_c)$ tends to increase for the two sets of molecules. The differences in the distributions of the valence electrons of the sulfide and oxide anions provide a basis for understanding why the crystal chemistries of sulfides and oxides are different and distinctive and why the sulfide anion has a greater tendency to form more directed, shared interaction bonds than the oxide anion. The directionality of Si-O and Si-S bonds and the compliances of the Si-S-Si and Si-O-Si bridging

TABLE 1. Bond critical point properties for sulfide molecules

Molecule	Bond	R(M-S)	r_b(S)	$\rho(r_c)$	λ_1	λ_2	λ_3	$\nabla^2\rho(r_c)$	$H(r_c)$
Li_4SiS_4	Li-S	2.629	1.814	0.103	−0.365	−0.177	2.325	1.783	0.014
Li_3BS_3	Li-S	2.253	1.506	0.189	−0.890	−0.856	5.189	3.443	0.014
$Li_3Al_3S_3$	Li-S	2.392	1.615	0.154	−0.673	−0.588	3.879	2.618	0.012
Li_2CS_3	Li-S	2.298	1.542	0.171	−0.807	−0.806	4.682	3.069	0.015
Li_2CS_3	Li-S	2.272	1.534	0.204	−1.016	−0.980	5.443	3.447	0.008
$LiNS_3$	Li-S	2.301	1.556	0.191	−0.960	−0.921	5.166	3.285	0.011
Li_8SiS_6	Li-S	2.371	1.592	0.147	−0.627	−0.597	3.926	2.703	0.017
$Mg^2Li_6MgS_6$	Li-S	2.495	1.684	0.116	−0.449	−0.435	2.887	2.003	0.014
$Mg_2Li_6MgS_6$	Li-S	2.470	1.671	0.128	−0.512	−0.495	3.223	2.216	0.014
$MgLi_7AlS_6$	Li-S	2.462	1.663	0.127	−0.515	−0.459	3.245	2.271	0.015
$MgLi_7AlS_6$	Li-S	2.434	1.641	0.134	−0.543	−0.523	3.453	2.388	0.016
$MgLi_7AlS_6$	Li-S	2.376	1.597	0.150	−0.638	−0.601	3.944	2.705	0.016
$MgLi_7AlS_6$	Li-S	2.466	1.659	0.119	−0.469	−0.437	3.034	2.129	0.015
$MgLi_7AlS_6$	Li-S	2.422	1.633	0.138	−0.573	−0.522	3.560	2.465	0.015
$H_6Li_3AlS_6$	Li-S	2.297	1.550	0.1944	−0.994	−0.892	5.206	3.320	0.012
Li_8SiS_6	Li-S	2.370	1.591	0.1473	−0.629	−0.599	3.942	2.714	0.017
Li_8CS_6	Li-S	2.311	1.546	0.1634	−0.750	−0.722	4.498	3.026	0.017
BeS	Be-S	1.726	1.184	0.7311	−3.237	−3.237	18.539	2.065	−0.332
Be_4S_4	Be-S	2.054	1.446	0.4220	−2.145	−2.080	8.768	4.512	−0.155
$Be_2Na_6MgS_6$	Be-S	2.073	1.459	0.403	−2.011	−2.011	8.177	4.155	−0.147
H_6BeS_4	Be-S	2.030	1.420	0.4147	−1.778	−1.778	8.857	5.300	−0.143
H_4BeS_4	Be-S	2.088	1.465	0.3506	−1.987	−1.797	7.960	4.176	−0.102
H_4BeS_4	Be-S	2.083	1.462	0.3548	−2.009	−1.829	8.061	4.222	−0.104
H_4BeS_4	Be-S	1.929	1.347	0.5712	−3.595	−3.225	11.947	5.127	−0.263
Li_3BS_3	B-S	1.854	1.284	0.987	−5.528	−5.028	3.175	−7.381	−1.013
Na_3BS_3	B-S	1.860	1.287	0.978	−5.486	−5.076	3.012	−7.550	−1.001
H_3BS_3	B-S	1.820	1.272	1.063	−6.387	−6.156	5.208	−7.334	−1.140
H_3BS_3	B-S	1.819	1.271	1.061	−6.370	−6.146	5.312	−7.204	−1.134
H_3BS_3	B-S	1.817	1.271	1.060	−6.373	−6.133	5.463	−7.044	−1.131
$H_4B_2S_5$	B-S	1.836	1.284	1.022	−6.175	−5.725	4.832	−7.068	−1.078
$H_4B_2S_5$	B-S	1.820	1.273	1.063	−6.363	−6.121	5.311	−7.173	−1.139
Li_2CS_3	C-S	1.773	0.855	1.285	−6.319	−5.745	4.977	−7.087	−0.936
Li_2CS_3	C-S	1.699	0.739	1.423	−6.567	−5.618	2.733	−9.451	−1.446
Na_2CS_3	C-S	1.769	0.851	1.289	−6.398	−5.788	4.972	−7.214	−0.946
Na_2CS_3	C-S	1.705	0.752	1.409	−6.605	−5.686	2.920	−9.371	−1.378
H_6C_2S	C-S	1.812	0.944	1.219	−6.584	−5.883	5.943	−6.524	−0.755
H_6C_2S	C-S	1.822	0.950	1.200	−6.443	−5.786	5.909	−6.319	−0.731
H_4CS_4	C-S	1.826	0.923	1.209	−6.549	−5.685	5.990	−6.244	−0.753
H_2CS_3	C-S	1.617	0.639	1.563	−6.601	−5.823	10.511	−1.913	−1.945
H_2CS_3	C-S	1.750	0.865	1.362	−7.848	−6.278	5.602	−8.524	−0.998
H_3NS_4	N-S	1.612	0.627	1.4047	−6.282	−5.711	18.803	6.811	−1.600
	N-S	1.738	0.724	1.2462	−6.962	−4.741	4.975	−6.727	−1.256
	N-S	1.618	0.630	1.3831	−6.105	−5.522	17.967	6.340	−1.565
	N-S	1.788	0.771	1.1433	−5.974	−4.653	4.824	−5.803	−0.986
H_5NS_5	N-S	1.786	0.748	1.0747	−5.486	−4.003	5.252	−4.237	−0.947
	N-S	1.779	0.744	1.0959	−5.670	−4.040	5.198	−4.511	−0.984
	N-S	1.780	0.744	1.0891	−5.607	−3.994	5.232	−4.368	−0.975
	N-S	2.506	1.321	0.3482	−1.194	−1.136	3.638	1.308	−0.057
$LiNS_3$	N-S	1.574	0.613	1.550	−7.808	−6.951	2.262	7.858	−1.864
	N-S	1.717	0.679	1.177	−4.760	−4.023	8.521	−0.262	−1.219
$NaNS_3$	N-S	1.584	0.616	1.520	−7.547	−6.689	2.140	7.168	−1.814
	N-S	1.712	0.677	1.186	−4.839	−4.120	8.770	−0.188	−1.235
HNS_3	N-S	1.606	0.624	1.4238	−6.474	−5.883	19.571	7.214	−1.632
	N-S	1.738	0.724	1.2456	−6.951	−4.738	4.977	−6.712	−1.255
	N-S	1.621	0.631	1.3725	−6.003	−5.429	17.592	6.159	−1.547
N_2S_5	N-S	1.786	0.748	1.0747	−5.486	−4.003	5.252	−4.237	−0.947
	N-S	1.779	0.744	1.0959	−5.670	−4.040	5.198	−4.511	−0.984
Na_4SiS_6	Na-S	2.872	1.758	0.093	−0.295	−0.178	2.049	1.576	0.016
Na_3BS_3	Na-S	2.593	1.555	0.153	−0.551	−0.540	3.755	2.665	0.018
Na_3AlS_3	Na-S	2.687	1.620	0.130	−0.437	−0.403	3.049	2.209	0.017
Na_2CS_3	Na-S	2.648	1.595	0.137	−0.510	−0.485	3.356	2.361	0.018
Na_2CS_3	Na-S	2.618	1.585	0.160	−0.617	−0.579	3.862	2.666	0.015
$NaNS_3$	Na-S	2.665	1.618	0.144	−0.599	−0.521	3.509	2.428	0.016
$Mg_2Na_6MgS_6$	Na-S	2.810	1.698	0.096	−0.295	−0.285	2.200	1.620	0.016
$Mg_2Na_6MgS_6$	Na-S	2.757	1.668	0.112	−0.359	−0.342	2.599	1.898	0.017
$Mg_2Li_6MgS_6$	Mg-S	2.656	1.683	0.168	−0.507	−0.481	3.446	2.458	0.002
$Mg_2Li_6MgS_6$	Mg-S	2.396	1.487	0.264	−0.979	−0.920	6.123	4.224	−0.010
$Mg_2Na_6MgS_6$	Mg-S	2.758	1.759	0.138	−0.408	−0.365	2.678	1.905	0.003
$Mg_2Na_6MgS_6$	Mg-S	2.390	1.481	0.266	−0.996	−0.924	6.156	4.236	−0.011
$MgLi_7AlS_6$	Mg-S	2.360	1.458	0.276	−1.041	−0.979	6.619	4.599	−0.009
H_6MgS_4	Mg-S	2.176	1.314	0.376	−1.281	−1.281	9.968	7.407	−0.024
Mg_4S_4	Mg-S	2.424	1.511	0.259	−0.961	−0.919	5.897	4.018	−0.012
$H_4Mg_2S_4$	Mg-S	2.452	1.523	0.220	−0.924	−0.843	5.294	3.527	0.001
$H_4Mg_2S_4$	Mg-S	2.453	1.524	0.219	−0.917	−0.839	5.270	3.514	0.001
$H_4Mg_2S_4$	Mg-S	2.303	1.424	0.338	−1.433	−1.244	8.022	5.345	−0.029

TABLE 1—*Continued*

Molecule	Bond	R(M-S)	r_b(S)	$\rho(r_c)$	λ_1	λ_2	λ_3	$\nabla^2\rho(r_c)$	$H(r_c)$
H_3AlS_3	Al-S	2.184	1.385	0.503	−2.362	−1.991	9.647	5.294	−0.180
Li_3AlS_3	Al-S	2.150	1.353	0.511	−2.029	−1.969	9.913	5.914	−0.180
Na_3AlS_3	Al-S	2.173	1.371	0.494	−2.017	−1.895	9.355	5.443	−0.173
H_9AlS_6	Al-S	2.469	1.599	0.280	−1.069	−1.014	4.733	2.651	−0.069
$MgLi_7AlS_6$	Al-S	2.764	1.808	0.179	−0.350	−0.344	1.962	1.268	−0.037
$H_6Li_3AlS_6$	Al-S	2.503	1.622	0.263	−0.959	−0.919	4.289	2.411	−0.063
$MgLi_7AlS_6$	Al-S	2.363	1.519	0.362	−1.310	−1.300	5.957	3.347	−0.112
Na_3AlS_3	Al-S	2.173	1.371	0.494	−2.017	−1.895	9.355	5.443	−0.173
H_9AlS_6	Al-S	2.469	1.599	0.280	−1.069	−1.014	4.733	2.651	−0.069
$MgLi_7AlS_6$	Al-S	2.764	1.808	0.179	−0.350	−0.344	1.962	1.268	−0.037
$H_6Li_3AlS_6$	Al-S	2.503	1.622	0.263	−0.959	−0.919	4.289	2.411	−0.063
$MgLi_7AlS_6$	Al-S	2.363	1.519	0.362	−1.310	−1.300	5.957	3.347	−0.112
Na_4SiS_6	Si-S	2.139	1.376	0.677	−2.678	−2.678	6.800	1.444	−0.457
Li_4SiS_4	Si-S	2.110	1.355	0.700	−2.762	−2.762	7.588	2.064	−0.474
Li_8SiS_6	Si-S	2.422	1.570	0.445	−1.334	−1.334	2.285	−0.384	−0.255
Na_8SiS_6	Si-S	2.482	1.590	0.408	−1.193	−1.193	1.468	−0.918	−0.220
H_6Si_2S	Si-S	2.156	1.389	0.631	−2.764	−2.625	7.069	1.680	−0.401
H_6Si_2S	Si-S	2.160	1.394	0.632	−2.756	−2.634	6.967	1.577	−0.403
H_4SiS_4	Si-S	2.142	1.383	0.689	−3.143	−2.840	7.152	1.169	−0.471
$(H_2Si_2S_3)_5$	Si-S	2.134	1.375	0.649	−2.724	−2.723	6.906	1.459	−0.422
$(H_2Si_2S_3)_5$	Si-S	2.140	1.379	0.643	−2.740	−2.631	6.726	1.355	−0.418
$(H_2SiS)_5$	Si-S	2.143	1.376	0.587	−2.492	−2.306	6.636	1.837	−0.353
$(H_3Si_2S_3)_2$	Si-S	2.148	1.385	0.659	−2.833	−2.757	6.906	1.316	−0.437
$(H_2SiS)_4$	Si-S	2.139	1.380	0.647	−2.741	−2.728	6.915	1.447	−0.416
$(H_6SiO)_6$	Si-S	2.160	1.389	0.596	−2.443	−2.419	6.245	1.383	−0.371
$(H_2SiO)_2$	Si-S	2.147	1.384	0.664	−2.866	−2.726	7.036	1.444	−0.442
$(H_2SiO)_2$	Si-S	2.152	1.388	0.651	−2.855	−2.717	6.903	1.330	−0.428
SiS_2	Si-S	1.906	1.188	0.091	−3.010	−3.010	11.420	5.401	−0.672
H_8SiO_6	Si-S	2.285	1.495	0.052	−1.686	−1.686	5.328	1.955	−0.316
Li_8SiS_6	Si-S	2.420	1.569	0.044	−1.340	−1.340	2.319	−0.362	−0.256
Na_8SiS_6	Si-S	2.479	1.589	0.041	−1.200	−1.200	1.505	−0.895	−0.222
HPS_3	P-S	1.891	1.000	1.2023	−4.668	−3.804	2.107	−6.365	−0.893
HPS_3	P-SH	2.067	1.160	0.9696	−4.508	−3.510	2.075	−5.943	−0.646
HPS_3	P-S	1.895	1.000	1.1924	−4.608	−3.776	2.171	−6.212	−0.877
H_5PS_5	P-Sa	2.270	1.282	0.7261	−2.892	−2.632	2.438	−3.087	−0.385
H_5PS_5	P-Se	2.110	1.148	0.9276	−4.098	−3.527	2.752	−4.873	−0.541
H_5PS_5	P-Se	2.113	1.158	0.9207	−4.051	−3.533	2.620	−4.964	−0.545

angles will next be examined in terms of the number and location of the local maxima in the VSCCs of the bridging anions.

Bonded and nonbonded maxima in the VSCCs of Si-S and Si-O bonds

In studies of molecular geometry and reactivity, Bader et al. (1984), Bader and MacDougall (1985), and MacDougall (1989) observed that the number and relative sizes of the maxima in the VSCC of a bonded atom, as determined by locating the extrema in the Laplacian {where $\nabla[\nabla^2\rho(\mathbf{r})] = 0$}, correspond one-to-one with the localized bonded and nonbonded pairs of electrons evoked in the Lewis and VSEPR electron pair models of the electronic structure of the atom (Lewis 1916; Gillespie and Hargittai 1991). A mapping of the extrema of the VSCCs of the bridging sulfide and oxide anions of the molecules $H_6Si_2S_7$ and $H_6Si_2O_7$ (calculated from wavefunctions generated at the Becke3LYP level) was undertaken, using the software BUBBLE, kindly supplied by Professor Richard Bader, to ascertain whether the narrower bridging angle (110.6°) of the former molecule can be related to lone electron pair—bond pair repulsions as done, for example, for the H_2S and H_2O molecules (Bader et al. 1984). Like the sulfide anion in H_2S, the bridging sulfide anion (S_{br}) of the $H_6Si_2S_7$ molecule is coordinated by a tetrahedral array of local concentrations of electron density ascribed to two nonbonded lone electron pair (lp) and two bonded electron pair (bp) concentrations of charge density at distances of 0.70 Å and 0.72 Å, respectively, from the sulfide anion; it is typical for lp electrons to be more tightly held and to be located slightly closer to the nucleus of an anion than bp electrons (Bader et al. 1984). The two lp concentrations of the molecule lie in a perpendicular plane that bisects the Si-S-Si angle and make an angle 132.0° at S_{br} whereas the two bp concentrations lie along the two Si-S bridging bonds making an angle of 109.3° at S_{br}. In this case, the path of the Si-S vector passes close to the bp concentrations of both Si-S bridging bonds. As expected from assertions made by Gillespie and Hargittai (1991), the angle between the local concentrations of charge density ascribed to the lone electron pairs (larger domains and space filling than bonded electron pair concentrations) is appreciably wider than that between bonded electron pairs. Given that the stereochemistry in the neighborhood of S_{br} is governed primarily by the repulsions among the electron pairs in its valence shell (Gillespie and Hargittai 1991), then the relatively stiff and narrow Si-S-Si angle adopted by the $H_2Si_6S_7$ molecule can be ascribed in part, as done for the H_2S molecule, to the strong repulsions that obtain among

the nonbonded and bonded electron pair charge concentrations in the valence shell of the sulfide anion.

The H_2O molecule, like the H_2S molecule, exhibits two lp concentrations and two bp concentrations, but its angle is ~10° wider than that in H_2S, suggesting that the lp-bp repulsions are greater for the latter molecule (Bader al. 1984), recalculated here at the Becke3LYP/6–311G(2d,p) level. The lp-O-lp angle calculated for H_20 is 134.0°, the lp-O-bp angle is 104.4° and the bp-O-bp angle is 101.0° whereas the distances between oxide anion and the lp and bp concentrations are 0.40 Å and 0.44 Å, respectively (see also Bader et al. 1984). However, only one lp and two bp concentrations were found in a search for the critical points of the VSCC of the bridging oxide anion (O_{br}) for a $H_6Si_2O_7$ molecule with C_{2v} point symmetry. In addition to the one lp on O_{br}, each of the nonbridging oxide anions of the molecule was found to display two lp charge concentrations (Fig. 3). The lp and the two bp concentrations, O_{br} and the two Si cations each lie in a common plane. The lp and bp pair concentrations coordinate O_{br} at the corners of a triangle such that <lp-O-bp = 106.4°, <bp-O-bp = 110.9° whereas the distances between O_{br} and the lp and bp concentrations are 0.35 Å and 0.37 Å, respectively. The bp concentrations do not, however, lie along the SiO_{br} bond vectors, but are each offset from the vectors toward the interior of the Si-O-Si angle (149.9°) by ~18°. The narrow angle in H_2O compared with that of the $H_6Si_2O_7$ molecule can be ascribed, at least in part, to the larger number of electron pair concentrations adopted in the VSCC of the former molecule. Deformation maps calculated in a perpendicular plane bisecting the Si-O-Si angle show a single peak in the vicinity of the lp concentrations. Maps calculated in the plane of the Si-O-Si angle of the molecule display a peak in the vicinity of each bp concentration offset from the Si-O bond vector toward the interior of the angle (Geisinger et al. 1987). However, we are at a loss to explain why the bridging oxide anion of the Si-O-Si unit displays only one lp whereas that of the water molecule displays two. Nonetheless, because there is only one lp and two bp concentrations and because the bp concentrations are offset from the Si-O bond vectors, the VSEPR theory would suggest that the constraints imposed on the stereochemistry of the Si-O-Si dimer by electron pair repulsions will be less restrictive on the geometry than if additional lp concentrations were present in the VSCC of the bridging oxide anion. Hence, the Si-O-Si angle can be expected to be less stiff and show a wider range of Si-O-Si angles as observed, with the Si-O bond being less directed than the Si-S bond because the repulsions among lp and the two bp concentrations will be less confining on the geometry (Geisinger and Gibbs 1981). However, the Si-O bond will be expected to exhibit a larger bond order than the Si-S bond because of the availability of the extra electron density that is left unused in the formation of a second lp concentration. Gillespie and Johnson (1997) observed in a study of disilyl ether that the Si-O bond is ''unusually short,'' which has been ascribed to a delocalization of the nonbonded electron density into the Si-O bond (Gillespie and Hargattai 1991). Despite the large displacement of the bp concentrations off the Si-O bond vectors toward the interior of the angle, it is noteworthy that the bond path closely parallels the vectors between Si and O, except near the nucleus of the bridging oxide anion (see below).

The displacement of the bp concentrations from the bridging Si-O vectors of the $H_6Si_2O_7$ molecule can be expected to result in a departure of the geometrical Si-O-Si angle of the molecule from the angle formed between the two bond paths that radiate from the bridging oxide anion. The difference, $\Delta\alpha = \alpha_b - \alpha_c$, between the geometrical Si-O-Si angle, α_c, for a molecule like $H_6Si_2O_7$ and the limiting angle between the two bond paths at the nucleus of the oxide anion (the bond path angle), α_b, has been used as a measure of the degree of relaxation of the electron density distribution from the geometrical constraints imposed on the molecule by its nuclear framework (Bader 1990). As found for a number of organic molecules, the greater the magnitude of $\Delta\alpha$, the greater the strain energy associated with the relaxation of the electron density distribution from each of their nuclear frameworks. The magnitude of the $\Delta\alpha$ value calculated for the Si-O-Si angle of the $H_6Si_2O_7$ molecule (|-6.6°|) is larger than that (|-3.3°|) calculated for the Si-S-Si angle of the $H_6Si_2S_7$. This difference can be ascribed in part to the greater displacement of the bonded electron pair charge concentration away from the bridging Si-O bond vectors of the molecule (~17° = < bpO-Si), in particular, toward the interior of the angle (see above) compared with that (~3°) calculated for the Si-S bond of the $H_6Si_2S_7$ molecule. This result suggests that the bridging Si-S-Si dimer is more strain free than the Si-O-Si dimer. It is noteworthy that the greater strain energy associated with the latter dimer can be related to deformation maps calculated for the molecules H_6Si_2O and H_6Si_2S (Gibbs et al. 1987a). The deformation map calculated for the Si-S-Si dimer of the H_6Si_2S molecule displays peaks of electron density that are centered on the Si-S vectors whereas that for the Si-O-Si dimer of the H_6Si_2O molecule shows a relatively large displacement of the peaks of electron density away from the Si-O bond vectors toward the interior of the Si-O-Si angle (Gibbs et al. 1987a). The bond path diverges significantly from the Si-O vector only in the vicinity of the bridging oxide anion.

The lp concentrations of the sulfur atom in the bisecting plane perpendicular to the H_2S molecule are at a greater distance from the nucleus and make a wider angle (~135°) at the sulfur atom than they make on the oxygen atom (~130°) of H_2O [calculated here at the Becke/6–311G(2d,p) level], demonstrating that the concentration of electron density in the lone pairs on sulfur is greater than that on oxygen (Bader et al. 1984). Also, the thickness and surface area of the lone pair concentrations on the sulfide anion, as defined by MacDougall (1989), are dramatically larger. These results suggest that the sulfide anion should be more prone to electrophilic attack than

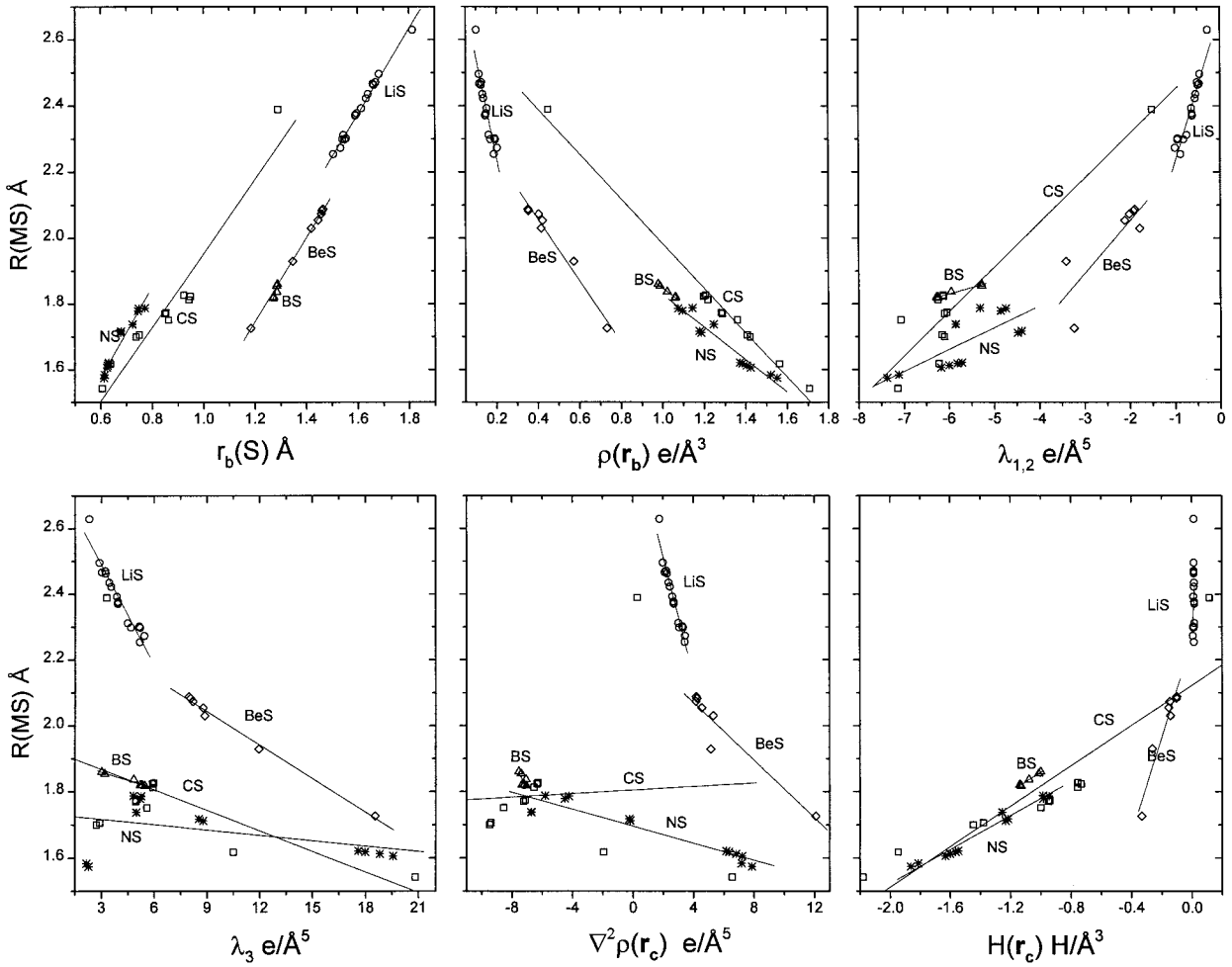

FIGURE 4. Scatter diagrams of the optimized bond length data, R(M-S), plotted against the bond critical point properties (Table 1) of the M-S bonds for the first-row M-cations Li, Be, B, C, and N: r_b(S) is the bonded radius of the sulfide anion; $\rho(\mathbf{r}_c)$ is the value of the electron density at the bond critical points, $\mathbf{r}_c$, $\lambda_{1,2}$ is the average curvature of the electron density perpendicular to the bond path at $\mathbf{r}_c$; λ_3 is the curvature of the electron density parallel to the bond path at $\mathbf{r}_c$; $\nabla^2\rho(\mathbf{r}_c)$ is the Laplacian of the electron density evaluated at $\mathbf{r}_c$ and $H(\mathbf{r}_c)$ is the local energy density of the electron density evaluated at $\mathbf{r}_c$. The open circles represent Li-S data, diamonds represent Be-S data, triangles represent B-S data, squares represent C-S data, and stars represent N-S data.

the oxide anion, all other things being equal (Bader and MacDougall 1985).

Bond critical point properties for M-S and M-O bonded interactions

In an exploration of the bcp properties of the sulfide bond and how they vary with bond length, the geometries of the sulfide molecules given in Table 1 were optimized at the Hartree-Fock/6–311G(2d,p) level. The resulting M-S bond lengths, R(M-S), together with the properties for each of the nonequivalent M-S bonds are given in the table. Earlier, Hill et al. (1997) and Rosso et al. (1998) found that the M-O bond lengths recorded for a number of oxide molecules and crystals provide a reliable measure of the bonded interactions, the shorter a given M-O bond, the greater the shared interaction of the bond. Similar results have been reported for the M-N bonds for a variety of nitride molecules (Feth et al. 1997). The length of the M-S bond length also provides a reliable measure of the shared bonded interaction. R(M-S) is plotted in Figure 4 for the first-row atoms M = Li, Be, B, C, and N and in Figure 5 for second-row atoms M = Na, Mg, Al, Si, and P against (1) $\mathbf{r}_b$(S), the bonded radius of the sulfide anion, (2) $\rho(\mathbf{r}_c)$, (3) $\lambda_{1,2} = 1/2(\lambda_1 + \lambda_2)$, (4) λ_3, (5) $\nabla^2\rho(r_c)$, the Laplacian of $\rho(\mathbf{r}_c)$ and (6) $H(\mathbf{r}_c)$, the local energy density (Bader 1990; Cremer and Kraka 1984). As the electronegativity of the M-cation increases from Na^+ to N^{+5}, R(MS) decreases from ~2.8 Å to ~1.6 Å, $\mathbf{r}_b$ (S) decreases from ~1.8 Å to ~0.6 Å, $\rho(\mathbf{r}_c)$ increases from ~0.1 e/Å^3 to 1.6 e/Å^3 and $\lambda_{1,2}$ decreases from ~−0.2 e/Å^5 to ~7.0 e/Å^5. With the exception of the P-S bond, λ_3 increases from ~3.0 e/Å^5 for the Na-S bond to ~8.0 e/Å^5 for the N-S bond accompanied by an increase in $\nabla^2\rho(\mathbf{r}_c)$. Unlike the remaining bond length data, as R(P-

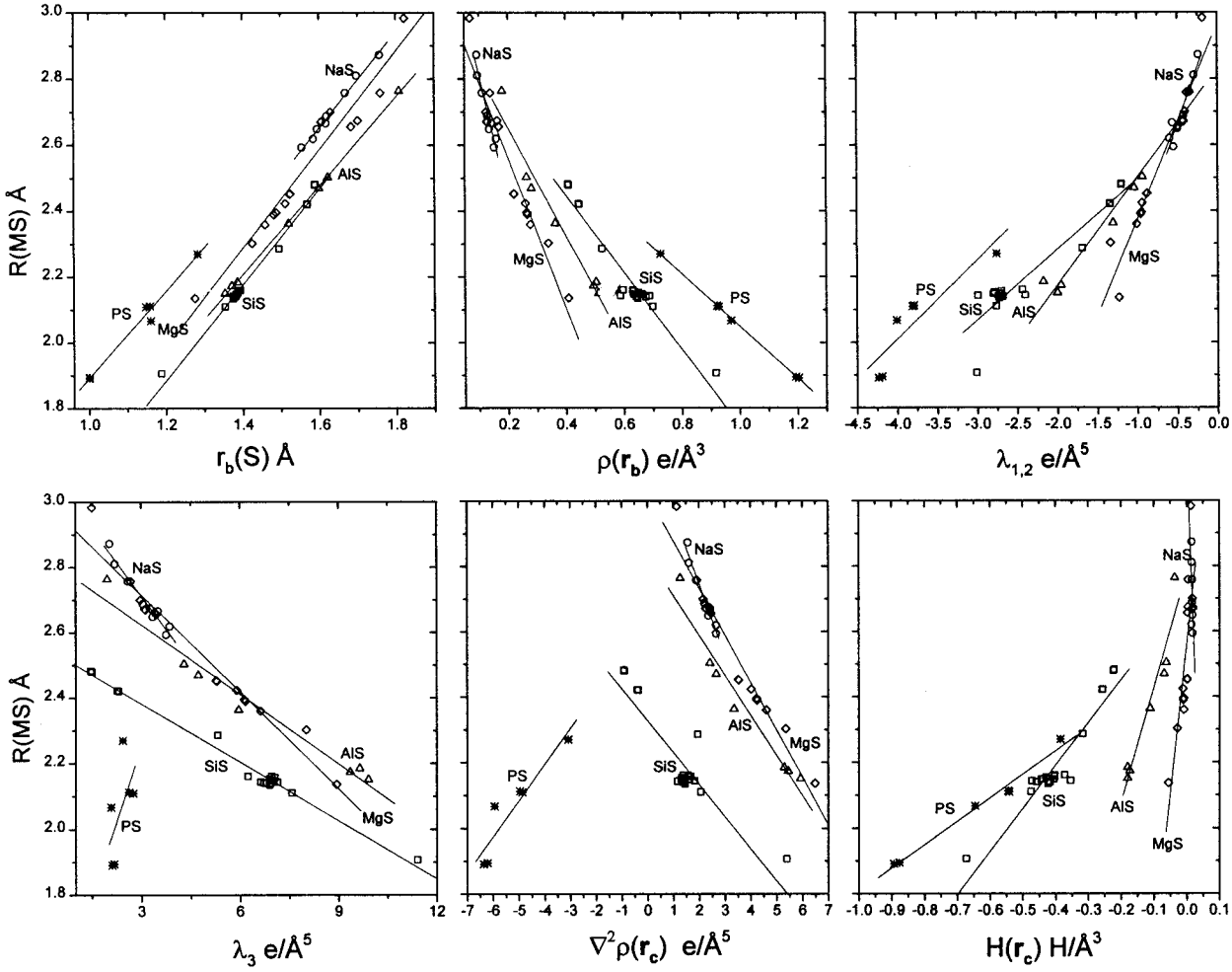

FIGURE 5. Scatter diagrams of R(M-S), plotted against the bond critical point properties (Table 1) of the M-S bonds for second-row M-cations Na, Mg, Al, S, and P: See Figure legend 4 for the definitions of R(M-S), r_b(S); $\rho(\mathbf{r}_c)$; $\lambda_{1,2}$; λ_3; $\nabla^2\rho(\mathbf{r}_c)$; and $H(\mathbf{r}_c)$. The open circles represent Na-S data, diamonds represent Mg-S data, triangles represent Al-S data, squares represent Si-S data and stars represent P-S data.

S) decreases, $\nabla^2\rho(\mathbf{r}_c)$ decreases and becomes more negative in value in accordance with the Bader-Essën (1984) rules for shared interactions. The reason for this difference lies in the near independence of λ_3 of R(P-S) accompanied with a concomitant decrease in the values of λ_1 and λ_2. In other words, with decreasing R(P-S), the curvatures of the electron density perpendicular to the bond path becomes progressively sharper whereas that along the bond remains essentially unchanged, resulting in a decrease in $\nabla^2\rho(\mathbf{r}_c)$. Nonetheless, as R(M-S) decreases, the value of $\rho(\mathbf{r}_c)$ increases, the curvatures of $\rho(\mathbf{r}_c)$ tend to increase and $\mathbf{r}_b$(S) decreases. Hence, as observed for oxide and nitrides, the shared interaction of a M-S bond increases as its bond length decreases. Not all of the trends in the figures are well developed. The data comprising the R(C-S) vs. $\nabla^2\rho(\mathbf{r}_c)$ trends show a wide scatter, indicating that R(C-S) is largely independent of this property. On the other hand, R(C-S) is highly correlated with the remaining bcp properties.

In a description of the chemical bond in terms of the local properties of the electron density and energy, Cremer and Kraka (1984) have suggested that covalent bonding requires the existence of a saddle point $\mathbf{r}_c$ of $\rho(\mathbf{r})$ in the internuclear region and a negative value for the local energy density $H(\mathbf{r}_c) = G(\mathbf{r}_c) + V(\mathbf{r}_c)$, where $G(\mathbf{r}_c)$ is the local kinetic energy density and where $V(\mathbf{r}_c)$ is the local potential energy density. In addition, they suggest that when $H(\mathbf{r}_c)$ is positive a non-covalent closed shell ionic interaction exists.

The value of $H(\mathbf{r}_c)$ in Figures 4 and 5 varies linearly with R(M-S), decreasing from ~0.01 Hartrees/Å^3 for the Na-S bonds to ~−2.0 Hartrees/Å^3 for the N-S bonds. As $H(\mathbf{r}_c)$ is positive in value for LiS, NaS, and MgS bonded interactions, they would be considered by Cremer and Kraka (1984) to be closed shell ionic interactions. The remaining interactions, which have negative $H(\mathbf{r}_c)$ values, would be considered to be bonded interactions with the shared interaction of the bonds increasing as $H(\mathbf{r}_c)$ de-

creases and $\rho(\mathbf{r}_c)$ increases in value. The local energy density for the M-S bonds involving first-row M cations are much more negative than that involving second-row cations. This conforms with observations made by Bader (1990) that first-row cations have a greater tendency to form shared interactions than second-row cations. Also, the general trend displayed in Figures 3 and 4 between R(M-S) and $H(r_c)$ is further evidence that the length of a bond provides a good measure of bond type, the shorter the bond, the greater its shared interaction.

Discussion

The variations in the bond critical point properties for sulfides, oxides, and nitrides show similar and consistent trends. With increasing electronegativity of the M cation from left to right in the periodic table, as a rule, the accumulation of electron density along the bond paths increases, bond lengths and bonded radii decrease and all three of the principal curvatures of $\rho(\mathbf{r})$ at $(\mathbf{r}_c)$ increase in magnitude. Also, the length of a given bond in sulfides, oxides, and nitrides is indicated to be a consistent signature of a bonded interaction, as observed by Brown and Shannon (1973) for the oxides, the shorter the bond, the greater its strength and the degree of its shared interaction.

By searching the VSCC of the sulfide and oxide anions, local maxima were found that provide a basis for understanding the stereochemistry of Si-S-Si and Si-O-Si bridging groups in terms of the VSEPR theory. It is noteworthy that the location of the local maxima (''lumps'') together with the location of the local minima (''holes'') in the VSCCs have been found by chemists to provide, for example, a basis for understanding the structure of acid-base reactions. According to Bader and MacDougall (1985), the approach of the reactants in a Lewis acid-base reaction can be predicted by aligning the lumps [(3,−3 critical points] in the VSCC of a base with the holes [(3,+3) critical points] in the VSCC of an acid. Thus, by locating the lumps and holes in the VSCCs of a mineral, a map of the sites of potential chemisorption and bacterial attack can be constructed. Such maps are bound to be useful to the mineralogists and geochemists in delineating those regions of a mineral surface that are potentially susceptible to electrophilic and nucleophilic attack (cf. Aray and Bader 1996 and references therein). Indeed, it is also anticipated that the maps will be useful in the construction of viable transition state structures and reaction paths in the study of reactions. Furthermore, their use may not only improve our understanding of the requirements for the activation of surface and internal oxide anions and catalysis in the zeolites, but also provide new and important insights into the role played by the functional groups that are potentially involved in mineral surface reactions with the organic ligands of microorganisms.

Acknowledgments

This paper is dedicated to Charles T. Prewitt on the occasion of his retirement as The Director of the Geophysical Laboratory and in celebration of his brilliant career as one of the top mineral physicists of our times.

We are pleased to thank Mark Bukowinski of the University of California at Berkeley and Jack Tossell of the University of Maryland for their thorough and helpful reviews of the manuscript and for making a number of valuable suggestions that definitely improved the manuscript. The National Science Foundation is thanked for generously supporting this study with grant EAR-9627458.

References cited

Aray, Y. and Bader, R.F.W. (1996) Requirements for activation of surface oxygen atoms in MgO using the Laplacian of the electron density. Surface Science, 351, 233–249.

Bader, R.F.W. (1990) Atoms in molecules. Oxford Science Publications Oxford, UK.

Bader, R.F.W. and Essén, H. (1984) The characterizations of atomic interactions. Journal of Chemical Physics, 80, 1943–1960.

Bader, R.F.W. and MacDougall, P.J. (1985) Toward a theory of chemical reactivity based on charge density. Journal of the American Chemical Society, 107, 6788–6795.

Bader, R.F.W., Nguyen-Dang, T.T., and Tai, Y. (1981) A topological theory of molecular structure. Report of Progress in Physics, 44, 893–947.

Bader, R.F.W., MacDougall, P.J., and Lau, C.D.H. (1984) Bonded and nonbonded charge concentrations and their relation to molecular geometry and reactivity. Journal of the Ameican Chemical Society, 106, 1594–1605.

Bartelmehs, K.L., Gibbs, G.V., and Boisen, Jr., M.B. (1989) Bond-length and bonded-radii variations in sulfide molecules and crystals containing main-group elements. American Mineralogist, 74, 620–626.

Brown, I.D. and Shannon, R.D. (1973) Empirical bond-strength bond-length curves for oxides, Acta Crystallographica, A29, 266–282.

Cremer, D. and Kraka, E. (1984) A Description of the Chemical Bond in Terms of Local Properties of Electron Density and Energy. Croatia Chemica Acta, 57, 1259–1281.

Feth S., Gibbs, G.V., Boisen, M.B., and Hill, F.C. (1998) A study of the bonded interactions in nitride molecules in terms of bond critical point properties and relative electronegativities. Physics and Chemistry of Minerals. 98, 234–241.

Frisch, M.J., Trucks, G.W., Schlegel, H.B., Gill, P.M.W., Johnson, B.G., Wong, M.W., Foresman, J.B., Robb, M.A., Head-Gordon, M., Replogle, E.S., Gomperts, R., Andres, J.L., Raghavachari, K., Binkley, J.S., Gonzalez, C., Martin, R.L., Fox, D.J., Defrees, D.J., Baker, J., Stewart, J.J.P., and Pople, J.A. (1993) Gaussian 92/DFT, Revision F.2 Gaussian Inc. Pittsburgh, PA.

Geisinger, K.L. and G.V. Gibbs (1981) SiSSi and SiOSi bonds in molecules and solids: A comparison. Physics and Chemistry and Minerals. 7, 204–210.

Geisinger, K.L., Spackman, M.A., and Gibbs, G.V. (1987) Exploration of structure, electron density distribution and bonding in coesite with Fourier and pseudoatom refinement methods using single crystal x-ray diffraction data. Journal of Physical Chemistry 91, 3237–3244.

Gibbs, G. V., P. D'Arco, and M.B. Boisen. (1987a) Molecular mimicry of bond length and angle variations in germanate and thiogermanate crystals: A comparison with variations calculated for C-, Si- and Sn-containing oxide and sulfide molecules. Journal of Physical Chemistry, 91, 5347–5354.

Gibbs, G.V., Finger, L.W. and Boisen, M.B. (1987b) Molecular mimicry of the bond length—bond strength variations in oxide crystals. Physics and Chemistry of Minerals, 14, 327–331.

Gibbs, G.V., Downs, J.W., and Boisen, M.B. (1994) The elusive SiO bond. Mineralogical Society of America Reviews in Mineralogy, 29, 331–368.

Gibbs, G.V., Hill, F.C., and Boisen, M.B. (1997) The SiO bond and electron density distributions. Physics and Chemistry of Minerals, 24, 167–178.

Gibbs, G.V., Boisen, M.B., Hill, F.C., Tamada, O., and Downs, R.T. (1998a) SiO and GeO bonded interactions as inferred from the bond critical point properties of electron density distributions. Physics and Chemistry of Minerals, in press.

Gibbs, G.V., Hill, F.C., Boisen, M.B., and Downs, R.T. (1998b) Power law relationships between bond length, bond strength and electron density distribution. Physics and Chemistry of Minerals, in press.

Gillespie, R.J. and Hargittai, I. (1991) The VSEPR Model of Molecular Geometry. Allyn and Bacon, Boston, MA, 1–248.

Gillespie, R.J. and Johnson, S.A. (1997) Study of bond angles and bond lengths in disiloxane and related molecules in terms of the topology of the electron density and its Laplacian. Inorganic Chemistry, 36, 3031–3079.

Hill, F.C., Gibbs, G.V., and Boisen, M.B. (1994) Bond stretching and force constants and compressibilities of nitride, oxide and sulfide coordination polyhedra in molecules and crystals. Structural Chemistry, 6, 349–355.

——— (1997) Critical point properties of electron density distributions for oxide molecules containing first and second row cations. Physics and Chemistry of Minerals, 24, 582–596.

Kaftory, M., Kapon, M., and Botoshansky, M. (1998) The structural chemistry of organosilicon compounds. In K. Rappoport and Y. Apeloig, Eds., The Chemistry of organic silicon compounds, Vol. 2, p. 181–265. Wiley, New York.

Kutzelnigg, W. (1984) Chemical bonding in higher group elements. Angewandte Chemie International. English edition, 23, 272–295.

Lewis, G.N. (1916) The atom and the molecule. Journal of the American Chemical Society, 38, 762–785.

Liebau, F. (1985) Structural chemistry of silicates. Springer-Verlag, Berlin, Germany

MacDougall, P.J. (1989) The Laplacian of the electron charge distribution, 128 p. Ph.D. Thesis, McMaster University.

Pauling, L. (1929) The principles determining the structure of complex ionic crystals. Journal of the American Chemical Society, 51, 1010–1026.

Rosso, K.M., Gibbs, G.V., and Boisen, Jr. M.B. (1998) SiO bonded interactions in coesite: A comparison of crystalline, molecular and experimental electron density distributions. Physics and Chemistry of Minerals, in press.

Wuench, B.J. (1974) Determination, relationships, and classification of sulfide mineral structures. Mineralogical Society of America Short Course Notes, 1, W1–W20.

Manuscript received March 26, 1998
Manuscript accepted October 7, 1998
Paper handled by Lars Stixrude